

**3D MODELING OF IRAN AND SURROUNDING AREAS FROM SIMULTANEOUS INVERSION OF
MULTIPLE GEOPHYSICAL DATASETS**

Charles J. Ammon¹, Monica Maceira², and Michael Cleveland¹

Penn State¹ and Los Alamos National Laboratory²

Sponsored by the Air Force Research Laboratory¹ and the National Nuclear Security Administration²

Award Nos. FA8718-09C-0007¹ and LA09-BAA09-12-NDD03²
Proposal No. BAA09-12

ABSTRACT

The objective of this work is to help improve seismic monitoring technology through the development and application of advanced multivariate inversion techniques to generate realistic, comprehensive, and high-resolution 3D models of the seismic structure of the crust and upper mantle that satisfy independent geophysical datasets. Our focus is on the region surrounding Iran from the east coast of the Mediterranean in the west, to Pakistan in the east, an area of prime importance to NEM, and a region with adequate calibration events to validate our model and to quantify its accuracy. Specifically, we are working to integrate surface-wave dispersion, receiver function, and satellite and ground-based gravity observations to help constrain the shallow seismic structure in the Arabian-Eurasian collision zone. Building on our earlier work combining receiver functions and surface wave dispersion, and surface-wave dispersion and gravity, we plan to continue to integrate geophysical data sets to create more broadly compatible earth models. We also explore geologically based smoothness constraints to help resolve sharp features in the underlying shallow 3D structure.

OBJECTIVES

The National Nuclear Security Administration (NNSA) and Air Force Research Laboratory (AFRL) have decided to investigate 3D modeling as part of the effort to improve knowledge of Earth's compressional and shear velocity structure. Such knowledge will help reduce uncertainty in our ability to accurately detect, locate, and identify small ($m_b \leq 3.5-4.0$) seismic events. For seismically active areas, with good ground-truth event coverage, earth models with limited accuracy can be corrected by interpolating results from nearby 'ground truth' events (using the kriging methodology) making it possible to detect, locate, and identify events even with limited resolution of Earth's structure. However, such approaches are less effective for smaller events, and event location and characterization remains a challenge for aseismic regions. To improve monitoring capability in such instances, we must develop better seismic earth models.

The objective of this work is to help improve seismic monitoring technology through the development and application of advanced multivariate inversion techniques to generate realistic, comprehensive, and high-resolution 3D models of the seismic structure of the crust and upper mantle that satisfy independent geophysical datasets. Our focus is on the region including and surrounding Iran (Figure 1) from the east coast of the Mediterranean in the west, to Pakistan in the east, a region with adequate calibration events to validate our models and to quantify their accuracy.

Background

Estimating subsurface geologic variations is a challenge. Seismologists have worked on the problem for more than a century (e.g., Milne, 1899; Macelwane and Sohon, 1936; Dahlen and Tromp, 1998). As data quantity has increased and data quality and computational ability have improved, we have made important advances in our understanding of the subsurface. Our best knowledge applies to the shallowest regions as well as depths with the sharpest global interfaces (sediment-basement contacts, the base of the crust, base of the mantle, and transitions near 410 km and 660 km depths), where resolution is improved as a result of the strong interactions of seismic body waves with sharp geologic transitions (e.g., Helmberger, 1968; Langston, 1979; Shearer, 1991; Lay et al., 2004). We have also done well modeling regions with smooth velocity changes such as the lower mantle, which allows us to exploit the information in teleseismic body-wave travel times to locate seismic sources reasonably well (e.g., Kennett, 2006). Still, many details within and just beneath the lithosphere elude us. We have been able to surmise that geologic variations here are substantial, and we know that they frustrate attempts to use robust observations such as regional seismic travel times to locate events in many parts of the Earth (e.g., Bondar et al., 2004).

Travel-time based tomography (e.g., Nolet, 2008) opened the doors to 3D imaging but the models remain blurry, often suffer from interpretational ambiguity, and are not easily used to predict other, independent seismic observations. From our own analyses (Maceira et al., 2005; Maceira and Ammon, 2009), we have seen how high-resolution surface-wave tomography fails to produce the extremes in seismic shear-wave speed that are evident from independent observations. In particular, achieving a model with low enough seismic wave speeds within the Tarim Basin to match seismograms from high-quality observations remains an issue. Waveform tomography methods improve the situation somewhat, including information from both the amplitude and phase of the signal, but restriction of these methods to lower frequency bands limits the resolution of the methods and the substantial computation requirements of these methods limit their application. More recent finite-frequency methods (e.g., Zhou et al., 2004; Dahlen and Zhou, 2006; Nolet, 2008) and adjoint methods (e.g., Tarantola, 1984; Tromp et al., 2008) offer more complete approaches to computing sensitivity kernels. But even these approaches face limits imposed by data bandwidth. In any event, such fully 3D waveform methods could benefit greatly from accurate, if approximate, starting models derived from more piecewise interpretation of seismic observables combined with other observations.

RESEARCH ACCOMPLISHED

Much of our effort during this project has been on the software development, although we have completed preliminary inversions that we present below with minimal discussion. At this point we caution readers about using or interpreting these preliminary earth models – they will improve as we explore various combinations of weighting for the different data sets and the appropriate configuration of geologic provinces that are consistent with the observations. We begin with a simple conceptual illustration of the challenges we address and conclude with a

discussion of accomplishments and plans for the final months of the project (exploring sensitivity by performing repeated inversions with various weight combinations inversions).

Combining Gravity, Rayleigh-Wave Dispersion, and P-wave Receiver Function Observations

Inversion of surface wave dispersion observations is a standard method for estimating 3D shear velocity structure of Earth's crust and upper mantle. Nevertheless, it is well known that traditional state-of-the-art inversion techniques suffer from poor resolution and nonuniqueness, especially when a single surface-wave mode is used (Huang et al., 2003). This is particularly true at shallow depths where the shorter periods, which are primarily sensitive to upper crustal structures, are difficult to measure, and especially true in tectonically and geologically complex areas. On the other hand, regional gravity inversions have the greatest resolving power at shallow depths since gravity anomalies decrease in amplitude and wavenumber bandwidth with increasing depth. Gravity measurements also supply constraints on rock density variations. Thus by combining surface-wave dispersion and gravity observations in a single inversion, we can obtain a self-consistent high-resolution 3D shear-velocity/density model with increased resolution of shallow geologic structures. Receiver function analysis (Langston, 1979) is a well-established tool for imaging relatively sharp changes in the subsurface structure that nicely complements information contained in surface-wave dispersion (e.g., Julia et al., 2000).

To improve our view of the earth structure within the focus region, we are working to combine receiver functions with surface-wave dispersion and gravity observations. The combination of receiver functions with tomographically localized surface-wave dispersion is well established (e.g., Julia et al. 2000). The integration of gravity observations with surface-wave dispersion is a more recent development (e.g., Maceira and Ammon, 2009), but these data are a good match. To a large part, the gravity observations add important constraints on the location of strong shallow heterogeneity to the information on smooth variations found in period-dependent dispersion maps. The choice of a density-velocity relationship can be subjective (Julia et al., 2004; Brocher, 2005; Maceira and Ammon, 2009), but testing the sensitivity of the results to a range of relations is not a challenge. To isolate gravity signatures associated with density variations (as opposed to dynamic and flexure variations) we plan to filter the gravity signals to include short wavenumbers sensitive to the crust. These concepts are summarized conceptually in Figure 2, which shows the regions of the lithosphere most sensitive to the different data that we employ.

To construct an approximate 3D model of the lithosphere, we use a hybrid 1D-3D inversion. In many tomography analyses, dispersion variations are converted to shear-velocity variations by inverting dispersion curves extracted from the tomographic model for a localized 1D structure. Smoothness constraints are applied to reduce cell-to-cell shear-velocity fluctuations in the resulting composite 3D structure. Since gravity observations can be efficiently modeled using prisms, they provide direct information on cell-to-cell density variations. In a particular cell surface wave dispersion can be inverted simultaneously with receiver functions (surface or downward-continued signals). In regions with receiver function overlap, multiple signals can be combined to produce a structure that matches compatible features in several receiver functions. Because of the hybrid nature of the inversion, the resulting model is an approximation to the true 3D structure, but we can still use it to provide a starting point for future full 3D waveform-based inversions of the subsurface.

Software Development Progress

A large component of the proposed work involves improving current software to allow more easy extension to larger focus areas and more flexible incorporation of additional data. For example, the earlier work in Maceira and Ammon (2009) blended gravity and surface-wave observations to produce a shear-velocity/density model for central Asia, but did not include receiver function information. Our inversion is a straightforward composite of coupled and uncoupled linearized inversions of nonlinear data and model relationships. In essence we construct a large set of coupled data and constrain equations into the form $Gm = d$, where the model parameters are in m , observations and constraint information is in d , and the system matrix, G , contains partial derivatives and coefficients of constraint equations.

The existing inversion tool used a singular value decomposition (SVD) to solve the system matrix, G . The SVD is a superb numerical choice for matrix inversion and problem analysis but the simplest implementations require substantial quantities of core memory and computational time increases rapidly as the problem grows large. To reduce these requirements we have replaced the SVD with Paige and Saunders (1982) LSQR conjugate-gradient based routine. We adopted the LSQR function from the Association for Computing Machinery (ACM) FORTRAN implementation last modified in 1994 (<http://toms.acm.org/>). Although well known to seismic tomographers (Pavlis, 1988; Nolet, 1993), the benefits of the LSQR algorithm may be less familiar to those working on multi-dataset

inversion tools. The key advantage is that the system matrix, G , need never be stored in memory. G can be stored on the disk as it is constructed one row at a time. The LSQR user need only develop a subroutine that computes $y = G y + y$ and $x = G^T x + x$, for vectors x and y provided during the inversion of G . G can be written to disk by saving only the nonzero columns of each row of the matrix and the associated indices of the nonzero columns. Not only do you save storage and input-output time, you also avoid waste by not multiplying numbers by zero. In our early experiments, we have saved roughly an order of magnitude in computation time (measured on a relatively simple desktop workstation). The great reduction in computation time allows more experimentation with and assessment of the model.

Example Rayleigh-Wave Dispersion Receiver Function Coupled Inversion

To illustrate the result of combining surface-wave dispersion and receiver functions in a coupled inversion of cells for an approximation to a 3D model, we selected a small, but interesting region of the focus area that includes the Caspian Sea. The Caspian Sea region is an area of complex geologic structure (e.g. Mangino and Priestly, 1998) and significantly low shear velocities. The sub region is shown in Figure 3, which also shows the misfit to the dispersion values for each cell. The dispersion values are from the University of Colorado tomographic effort (Ritzwoller and Levshin, 1998; Levshin et al., 2001, 2002). The initial misfits are large, but the inversion converges nicely to reasonable fits after four iterations (final). Two depth slices of the corresponding shear-velocity model (initial and final) are shown in Figure 4. The interpolation and contouring algorithm had some trouble with the rough initial model that contained two structures, one for region within the Caspian Sea and another for the rest of the model. We applied a simple Laplacian smoothing between adjacent cells so the resulting model remains smooth.

Next, we added one receiver function to the dispersion data and repeated the 3D shear-velocity inversion. The receiver function was digitized from Mangino and Priestly (1998), and samples the structure in our cell with the lower left corner at 53E and 40N (Figure 5). Figure 5 is a plot of the initial and final dispersion fits, which show little change from those without the receiver function. The initial and final fit to the receiver function are shown in Figure 6. The effect of including the receiver function is to thicken the crust and better define the crust-mantle boundary. The net result is a decrease in the velocity at the depth slice near 37 km. Two depth slices of the corresponding shear-velocity model (initial and final) are shown in Figure 7. The thickening of the crust near the receiver function observation is clearly visible in the deeper slice through the model (compare Figure 4 and Figure 7). The fit to the receiver function is not perfect and the spread of the slower deep crustal speeds into the Caspian region does not make sense geologically. These effects are driven by the simple Laplacian smoothness requirements placed on the 3D model.

Including Geologic Information

To produce models that have realistic ‘sharp’ boundaries requires that we include independent information on the location of those boundaries. Such information is available (for the shallow part of the model) in independent data sets such as gravity, surface geologic maps, and even something as simple as topography. As part of this work, we plan to resolve sharp features by adapting our imaging algorithms to allow the inclusion of geologic information on the location and nature of the boundary into shear-velocity inversions that permit such features (implemented through custom geologic smoothness constraints that allow velocities to be de-correlated across major geologic transitions). Including a priori information into an inversion is obviously only as good as the information that is included. Thus the inclusion of this type of information into the reconstruction of shear-velocity models of the subsurface must proceed carefully and include documentation of the importance of the assumed a priori information on the resulting model. Implementation of these smoothing constraints requires more work, but in the end includes more information in the shear-velocity model reconstruction, and hopefully leads to improved regional earth models.

Preliminary Application to the Iranian Plateau and Surrounding Regions

Our inversion is a straightforward composite of coupled and uncoupled linearized inversions of nonlinear data and model relationships. The preliminary results we present below do not yet include the gravity variations. We are working on adding spatial filtering of the gravity to the inversion so that we can focus on shallow lateral density variations and not map broad gravitational variations that may also be related the effects of the dynamic support of loads into lateral variations in structure. Since these are preliminary results, we invest little space interpreting the variations. We relied on the dispersion models from the University of Colorado group (Ritzwoller and Levshin, 1998; Levshin et al., 2001, 2002) and group and phase velocity estimates from the Harvard study (Ekström et al., 1997; Larson and Ekström, 2001; Dalton and Ekström, 2006) for the results shown in this section. We started the

2011 Monitoring Research Review: Ground-Based Nuclear Explosion Monitoring Technologies

inversion using only Rayleigh-wave dispersion (group velocities from the Colorado model and phase velocities from the Harvard studies) in the period range from 7 to 200 seconds (with more weight on the shorter periods).

The results for the broad study region are shown in Figures 8, 9, and 10. We show depth slices of the models for two levels of smoothing. The results incorporate information from geologic province-based constraints that include oceanic regions, the South Caspian, North Caspian, the Persian Gulf, the Mesopotamian foredeep, the Arabian shield, the Zagros, etc. as separate areas. Increasing the smoothing requirements produces fewer variations within the geologically defined regions, but can produce sharper edges between the boundaries (Figure 8). In most regions (depending on the structure), the depth slices correspond to upper, middle, and lower crust, and upper mantle. Note that the velocity scale changes with each depth. The shallow structure is dominated by basins with thick sediments (as was clear in earlier inversion by the Colorado group). In general, in the preliminary model, the Zagros crust is relatively slow, compared with central Iran and the platform to the north and east. The upper mantle is generally slow across the entire region. The slowest material correlates reasonably well with volcanic centers (Figure 1). Figure 8 is neither a comprehensive exploration of the model, nor can we see all the features that we might expect.

We included receiver function constraints in the inversion in two ways. The first is a straightforward inclusion of observed receiver functions. Not all receiver functions map simply into one-dimensional velocity structures and in many cases individual researchers have invested substantial effort to extract approximate one-dimensional structures compatible with observed receiver functions of varying complexity (Doloei and Roberts, 2003; Paul et al., 2006; Gök et al., 2007; Pasyanos et al., 2007; Gök et al., 2008; Taghizadeh-Farahmand et al., 2010; Asfari et al., 2011). We have used the results to construct synthetic receiver functions from the resulting one-dimensional structures and included those signals in the inversion in place of the original observations (which, frankly are also not always available or not always easily digitized from the published results). The “observed” and predicted receiver functions for the middle, “smooth”, model of Figure 8 are shown in Figure 9. Panels with a title beginning with the word model identify those constraints that are constructed using a model from the literature, not a direct observation. We associate each receiver function with a 1° cell and ignore the few cases where the sampling may be across several cells. Smoothing will account for some of the complexities associated with that situation, and examination of the station and receiver function geometry suggests that most of the receiver functions are likely sampling only a single cell. In general the fits are quite good, even for some of the complex receiver functions associated with thick sedimentary sequences such as KUW1, Kuwait, from Pasyanos et al. (2007).

The dispersion misfits for the “smooth” model of Figure 8 are shown in Figure 10. In general the fits are reasonable (as measured by a single misfit norm). However, we have not yet explored the potential for systematic misfits that vary with period, observations type group vs. phase, etc. Understanding and estimating the robustness of the shear-velocities will require this level of model and fit assessment. Our work continues on adding the surface-gravity observations to these data and expanding the receiver function and surfaces waves included in the inversions.

CONCLUSIONS

We are completing our two-year project to map the subsurface geologic variations using seismic dispersion, gravity, and receiver-function observations. We faced significant challenges in our efforts to include effective point constraints on structure (receiver functions) with the spatially continuous surface-wave tomography and gravity observations. Our work complements ongoing work at LANL to integrate body-wave travel times into the same formalism. Our basic philosophy is that models that explain more data are better. The ultimate utility of the derived earth models is to provide improved predictive capabilities for routine seismic analyses and to provide adequate starting models for 3D waveform inversion approaches.

ACKNOWLEDGEMENTS

We thank the scientists, engineers, and technicians that have created the seismic-recording systems and networks that provide excellent broad-band seismic observations. In particular, we thank the USGS and the IRIS Consortia (NSF) who share information and data with the global community in an effective and efficient manner. We also thank the many international groups involved in collecting and sharing quality seismic observations. We also thank Wessel and Smith (1991), the developers of the Generic Mapping Tools software, which we use to create many of the illustrations of our research. Rengin Gök graciously provided us with her receiver functions models. Our thanks to M. Wetovsky for editorial assistance.

REFERENCES

- Afsari, N., F. Sodoudi, F. Taghizadeh-Farahmand, and M. R. Ghassemi (2011), Crustal structure of Northwest Zagros (Kermanshah) and Central Iran (Yazd and Isfahan) using teleseismic Ps converted phases, *J Seismol. Soc. Am.*, 15(2): 341–353, doi:10.1007/s10950-011-9227-x.
- Bondar, I., S. C. Myers, R. E. Engdahl, and E. A. Bergman, (2004). Epicentre accuracy based on seismic network criteria, *Geophys. J. Int.*, 156: 483–496.
- Brocher, T. A. (2005), Empirical relations between elastic wavespeeds and density in the earth's crust, *Bull. Seismol. Soc. Am.*, 95(6), 2081–2092.
- Dahlen, F. A., and J. Tromp (1999). *Theoretical Global Seismology*. Princeton University Press, Princeton, NJ, 1025 pp.
- Dahlen, F.A. and Y. Zhou (2006), Surface-wave group-delay and attenuation kernels, *Geophys. J. Int.*, 165, 545–554.
- Dalton, C. A., and G. Ekström (2006), Constraints on global maps of phase velocity from surface-wave amplitudes, *Geophys J Int*, 167(2): 820–826, doi:10.1111/j.1365-246X.2006.03142.x.
- Doloei, J., and R. Roberts (2003), Crust and uppermost mantle structure of Tehran region from analysis of teleseismic P-waveform receiver functions, *Tectonophysics*, 364, 115–133, doi:10.1016/S0040-1951(03)00049-0.
- Ekström, G., J. Tromp, and E. W. F. Larson (1997), Measurements and global models of surface wave propagation, *J Geophys Res*, 102(B4), 8137–8157, doi:10.1029/96JB03729.
- Gök, R., M. E. Pasyanos, and E. Zor (2007), Lithospheric structure of the continent-continent collision zone: eastern Turkey, *Geophys J Int*, 169(3), 1079–1088, doi:10.1111/j.1365-246X.2006.03288.x.
- Gok, R., H. Mahdi, H. Al-Shukri, and A. J. Rodgers (2008), Crustal structure of Iraq from receiver functions and surface wave dispersion: implications for understanding the deformation history of the Arabian-Eurasian collision, *Geophys J Int*, 172(3): 1179–1187, doi:10.1111/j.1365-246X.2007.03670.x.
- Helmberger, D. (1968). The crust-mantle transition in the Bering Sea, *Bull. Seismol. Soc. Am.*, 58: 179–214.
- Huang, Z., W. Su, Y. Peng, Y. Zheng, and H. Li (2003). Rayleigh wave tomography of China and adjacent regions, *J. Geophys. Res.*, 108, doi:10.1029/2001JB001696.
- Julia, J., C. J. Ammon, R. B. Herrmann, and A. M. Correig (2000), Joint inversion of receiver function and surface wave dispersion observations, *Geophys. J. Int.*, 143: 1–19.
- Julia, J., R. B. Herrmann, C. J. Ammon, and A. Akinici (2004), Evaluation of deep sediment velocity structure in the New Madrid Seismic Zone, in *Bull. Seismol. Soc. Am.*, edited, pp. 334–340.
- Kennett, B. L. N. (2006). Non-linear methods for event location in a global context, *Phys. Earth Planet. Int.*, 158, 46–54.
- Langston, C. A. (1979). Structure under Mount Rainier, Washington, inferred from teleseismic body waves, *J. Geophys. Res.*, 84, 4749–4762.
- Larson, E. W. F., and G. Ekström (2001), Global Models of Surface Wave Group Velocity, *Pure Appl Geophys*, 158(8), 1377–1399, doi:10.1007/PL00001226.
- Lay, T., E. J. Garnero, and S. Russell (2004). Lateral variation of the D'' Discontinuity beneath the Cocos Plate, *Geophys. Res. Lett.*, 31: L15612, doi:10.1029/2004GL020300.

2011 Monitoring Research Review: Ground-Based Nuclear Explosion Monitoring Technologies

- Levshin, A. L., M. H. Ritzwoller, M. P. Barmin, and J. L. Stevens (2001), Short period group velocity measurements and maps in central Asia, paper presented at the 23rd Seismic Research Review: Worldwide Monitoring of Nuclear Explosions, Natl. Nucl. Secur. Admin., Jackson Hole, Wyo.
- Levshin, A. L., J. L. Stevens, M. H. Ritzwoller, and D. A. Adams (2002), Short-period (7-s to 15-s) group velocity measurements and maps in central Asia, paper presented at the 24th Seismic Research Review– Nuclear Explosion Monitoring: Innovation and Integration, Natl. Nucl. Secur. Admin., Ponte Vedra Beach, Fla.
- Liang, C., X. Song, and J. Huang (2004). Tomographic inversion of Pn travel times in China, *J. Geophys. Res.*, 109, B11304, doi:10.1029/2003JB002789.
- Maceira, M. and C. J. Ammon (2009). Joint Inversion of Surface Wave Velocity and Gravity Observations and its Application to Central Asian Basins Shear Velocity Structure, *J. Geophys. Res.*, 114, B02314, doi:10.1029/2007JB005157.
- Maceira, M., S. R. Taylor, C. J. Ammon, X. Yang (2005). High-resolution Rayleigh wave slowness tomography of central Asia, *J. Geophys. Res.*, 110, doi:10.1029/2004JB003429.
- Macelwane, J. B. and F. W. Sohon (1936). *Introduction to Theoretical Seismology, Part I, Geodynamics*. John Wiley and Sons, Inc., New York, 336 pp.
- Mangino, S., and K. Priestley (1998), The crustal structure of the southern Caspian region, *Geophysical Journal International*, 133(3), 630-648.
- Milne, J. (1899). *Earthquakes and Other Earth Movements* (4th Edition). D. Appleton and Company, New York, 376pp.
- Nolet, G. (1993), Solving large linearized tomographic problems, in *Seismic Tomography - Theory and Practice*, edited by H. M. Iyer and K. Hirahara, pp. 227-247, Chapman & Hall, London.
- Nolet, G. (2008), *A breviary of seismic tomography : imaging the interior of the earth and sun*, xiv, 344 p. pp., Cambridge University Press, Cambridge, UK ; New York.
- Paige, C. C., and M. A. Saunders (1982), LSQR: An algorithm for sparse linear equations and sparse least squares, *ACM Trans. Math. Softw.*, 8, 43-71.
- Paul, A., A. Kaviani, D. Hatzfeld, J. Vergne, and M. Mokhtari (2006), Seismological evidence for crustal-scale thrusting in the Zagros mountain belt (Iran), *Geophys J Int*, 166(1), 227–237, doi:10.1111/j.1365-246X.2006.02920.x.
- Pasyanos, M. E., H. Tkalcic, R. Gok, A. Al-Enezi, and A. J. Rodgers (2007), Seismic structure of Kuwait, *Geophys J Int*, 170(1), 299–312, doi:10.1111/j.1365-246X.2007.03398.x.
- Pavlis, G. L. (1988), Vector and matrix manipulation algorithms, in *Seismological Algorithms, Computational Methods and Computer Programs*, edited by D. J. Doornbos, pp. 403-426, Academic Press Limited, San Diego, CA.
- Ritzwoller, M. H., and A. L. Levshin (1998), Eurasian surface wave tomography: Group velocities, *J. Geophys. Res.*, 103, 4839–4878.
- Shearer, P. M. (1991). Constraints on upper mantle discontinuities from observations of long-period reflected and converted phases, *J. Geophys. Res.*, 96, 18147-18182.
- Taghizadeh-Farahmand, F., F. Sodoudi, N. Afsari, and M. R. Ghassemi (2010), Lithospheric structure of NW Iran from P and S receiver functions, *J Seismol*, 14(4), 839–839, doi:10.1007/s10950-010-9206-7.
- Tarantola, A. (1984). Inversion of seismic reflection data in the acoustic approximation, *Geophysics*, 49, 1259-1266.

2011 Monitoring Research Review: Ground-Based Nuclear Explosion Monitoring Technologies

- Tromp, J., D. Komatisch, and Q. Liu (2008). Spectral-element and adjoint methods in seismology, *Communications in Comp. Physics*, 3, 1-32.
- Wessel, P., and W. H. F. Smith (1991), Free software helps map and display data, *EOS, Trans. of Am. Geophys. Union*, 72, 441,445.
- Zhou, Y. F. A. Dahlen, G. Nolet, G. Laske (2004). Finite-frequency effects in global surface-wave tomography, *Geophys. J. Int.*, 163, 1087-1111.

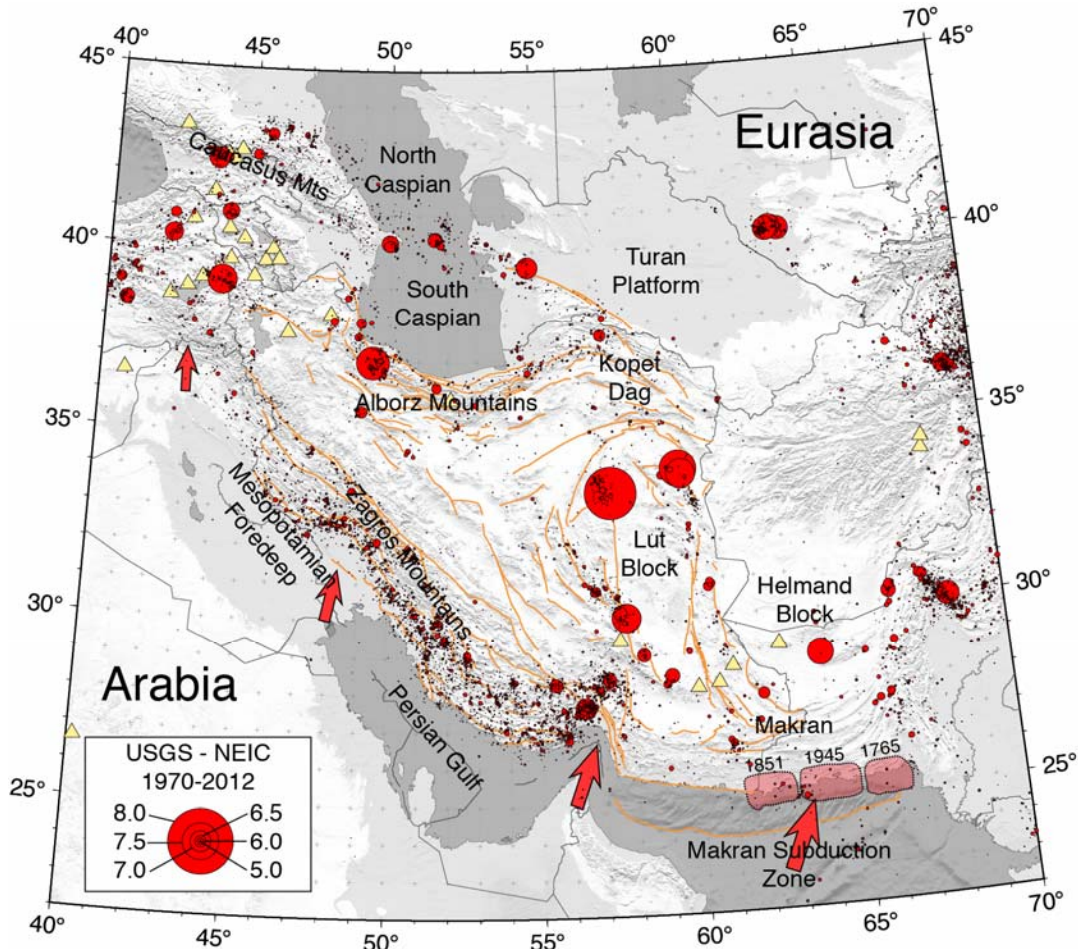


Figure 1. Map of focus region shown with topographic and bathymetric shading and moderate to large earthquake locations (magnitudes ≥ 4.0 from 1973 to Spring, 2011). The region contains the Arabian plate and the middle segment of the Alpine to Himalyan collision zone, which is constructed primarily of Phanerozoic terranes amalgamated onto southern Eurasia during the closing of the Tethys Ocean. Seismicity is shown using red circles, and the area of the circle is proportional to the event moment and represents roughly the area expected to have ruptured in an event of that size. Large historic subduction zone events are shown as rectangles. Faults within Iran are shown as orange lines, and quaternary volcanic centers are shown as yellow triangles. Red arrows show the motions of Arabia relative to Eurasia.

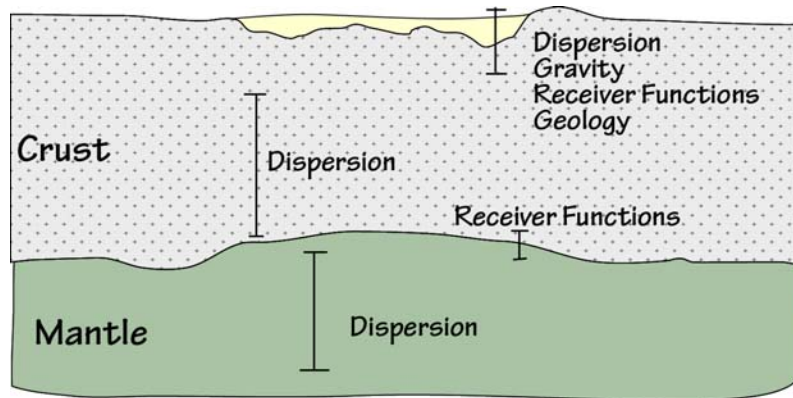


Figure 2. Conceptual illustration of the primary sensitivities of different data sets to the different depths of the lithosphere in a simultaneous inversion of surface-wave dispersion, gravity, and receiver-function observations. The crust shown contains a large basin (yellow). The receiver functions provide information on strong velocity contrasts such as the crust-mantle transition and near-surface structures; the spatially filtered gravity provides constraints on near-surface structures; and dispersion provided information on the absolute seismic velocities throughout the structure. Note that this cartoon is conceptual; the sensitivity of the data is more subtle than shown.

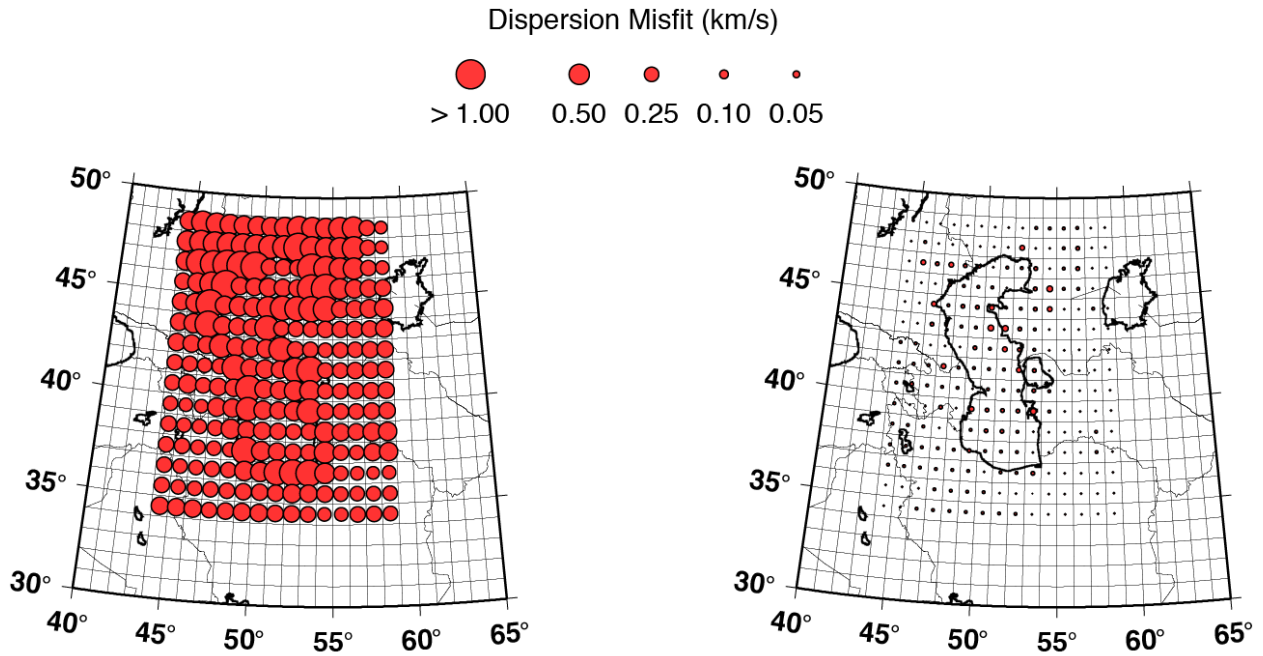


Figure 3. Initial (left) and final (right) dispersion misfit associated with the example subregion inversion of dispersion only. The initial model consists of a simple “continental” model and a Caspian Sea model. The initial misfits are large, but the convergence is reasonable to mean misfit values near or below 0.05 km/s. The cell containing the isolated receiver function is labeled.

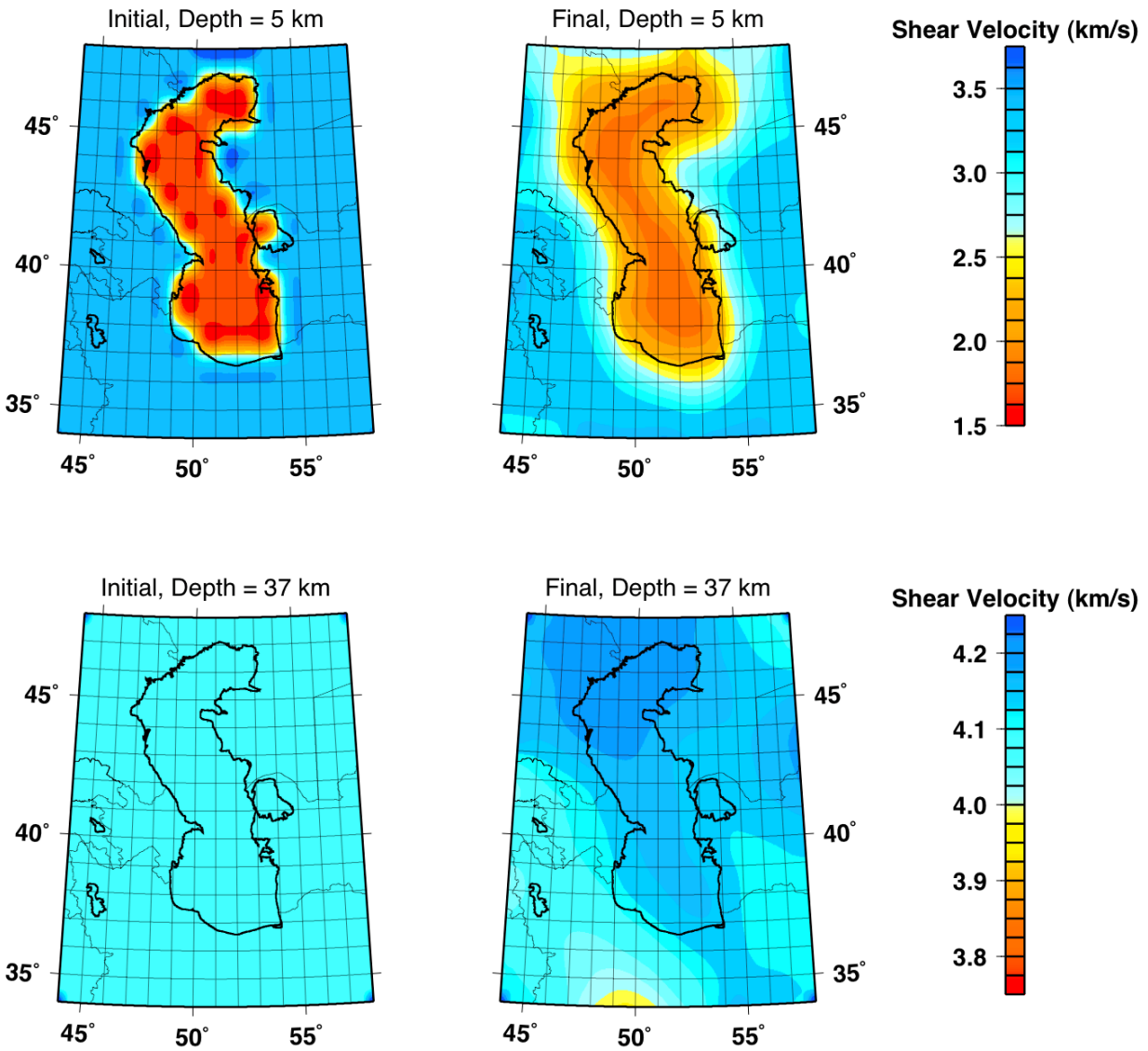


Figure 4. Initial (left) and final (right) shear-velocity values associated with the example subregion inversion of dispersion only for the upper and lower crust or upper mantle region of the model. The interpolation distorts the rough initial model producing artifacts that are absent when the inversion is complete and the model is smoother (we use a 1° cell dimension for the inversion).

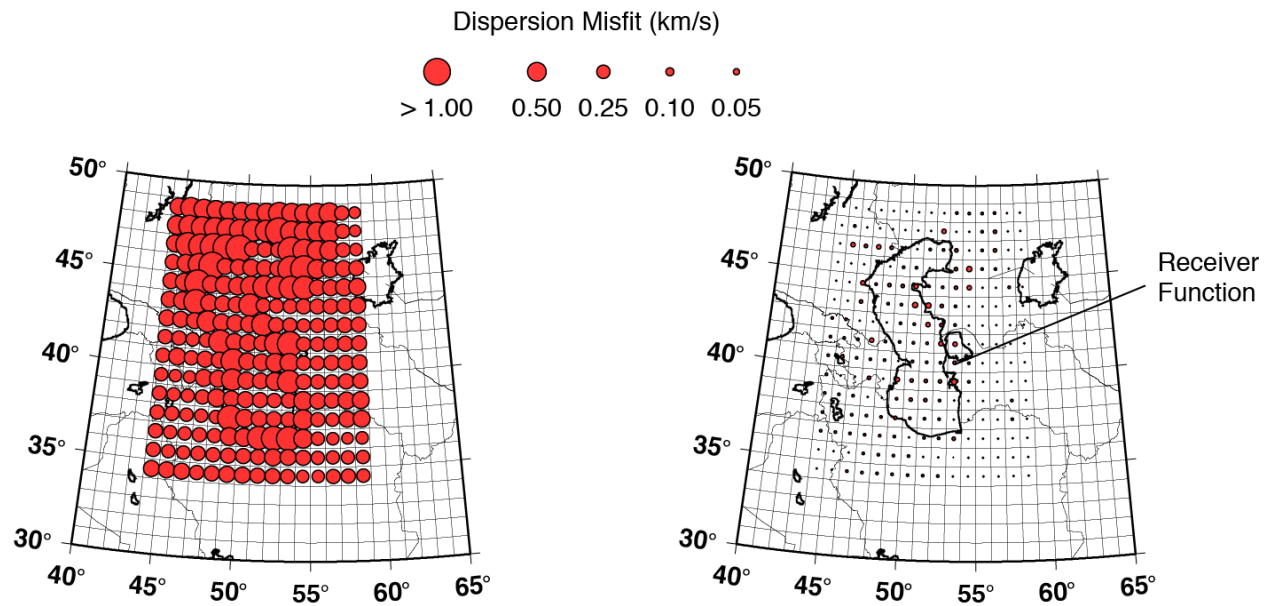


Figure 5. Initial (left) and final (right) dispersion misfit associated with the example subregion inversion of dispersion and a receiver function. The initial model consists of a simple “continental” model and a Caspian Sea model. The initial misfits are large, but the convergence is reasonable to mean misfit values near or below 0.05 km/s. The cell containing the isolated receiver function is labeled.

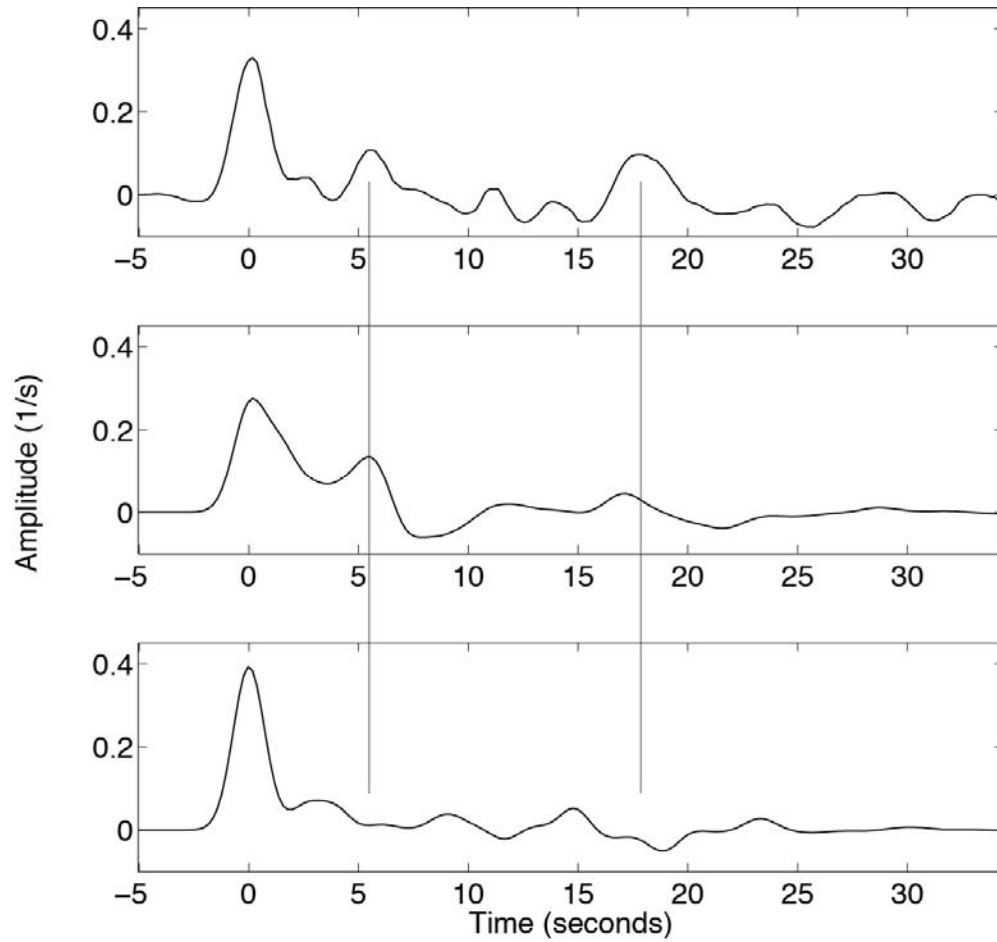


Figure 6. Observed (top), final prediction (middle) and initial prediction (bottom) of the receiver function from the inversion shown in Figure 5. Vertical lines show the arrivals most likely associated with the crust-mantle transition. Although the final fit is certainly not perfect, note the improvement in timing of the main crustal conversion and reverberation (vertical lines) from the initial to final models.

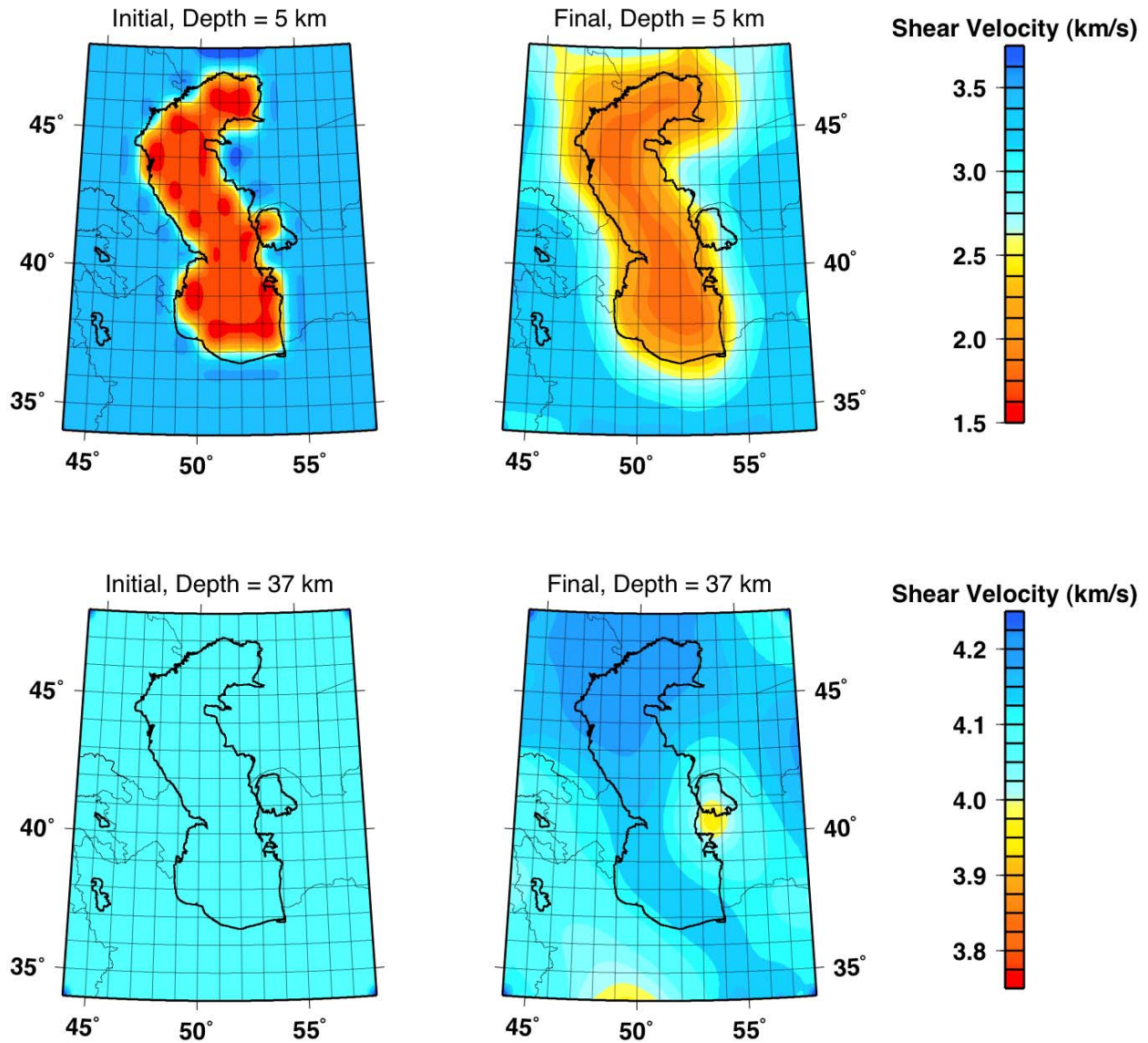


Figure 7. Initial (left) and final (right) interpolated shear-velocity values associated with the example subregion inversion of dispersion and a receiver function for the upper and lower crust or upper mantle region of the model. The cell containing the isolated receiver function has a lower left corner at 40N, 53E. The addition of the receiver function improves the estimate of crustal details. Please note the dramatic difference in the velocity scales shown to the right of each pair of images. The interpolation distorts the rough initial model producing artifacts that are absent when the inversion is complete and the model is smoother (we use a 1° cell dimension).

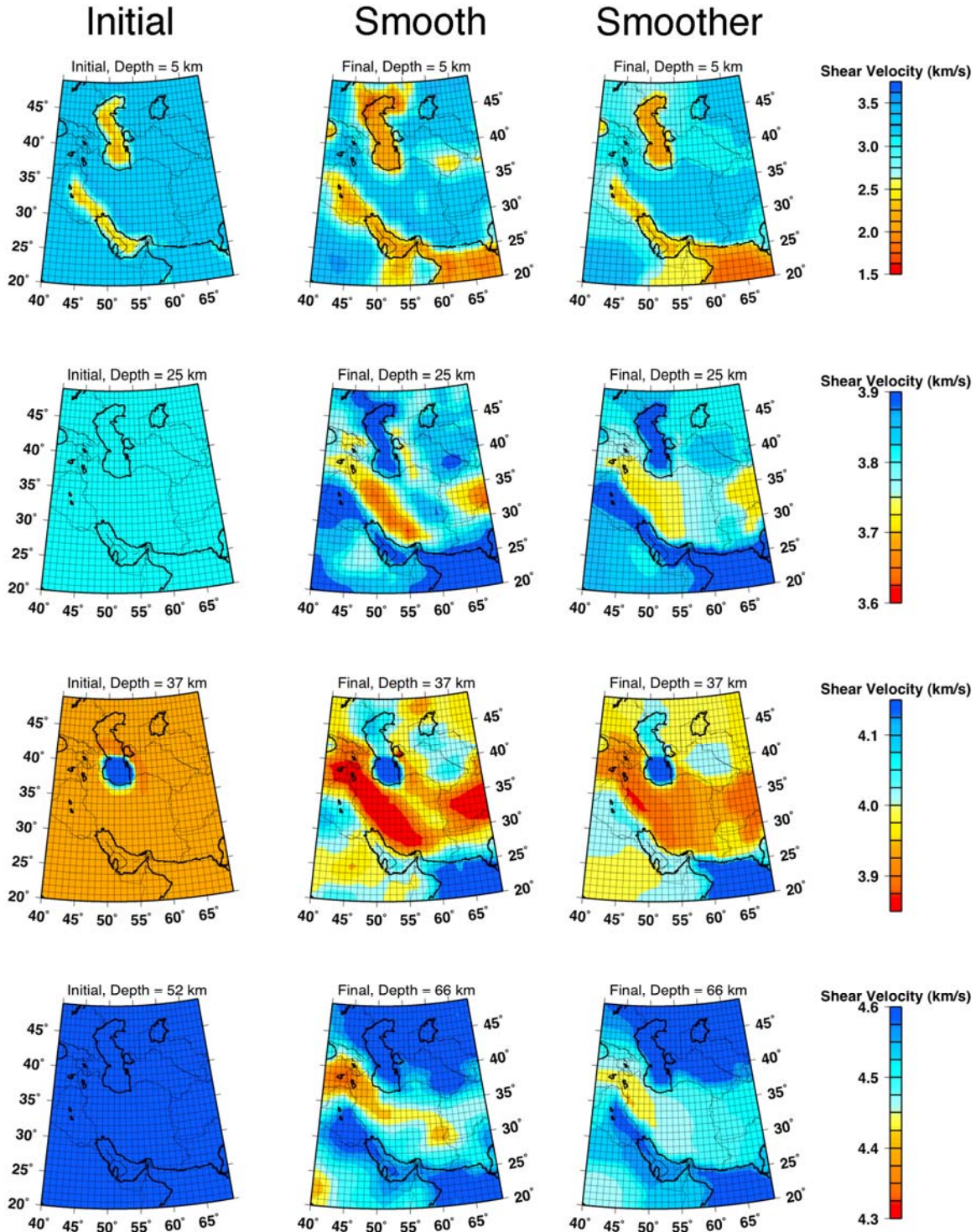


Figure 8. Initial (left) and two sample inversion results using just Rayleigh group and phase velocities combined with 13 receiver functions. Please note the significant difference in the velocity scales shown to the right of each pair of images. The interpolation distorts the rough initial model producing artifacts that are absent when the inversion is complete and the model is smoother (we use a 1° cell dimension).

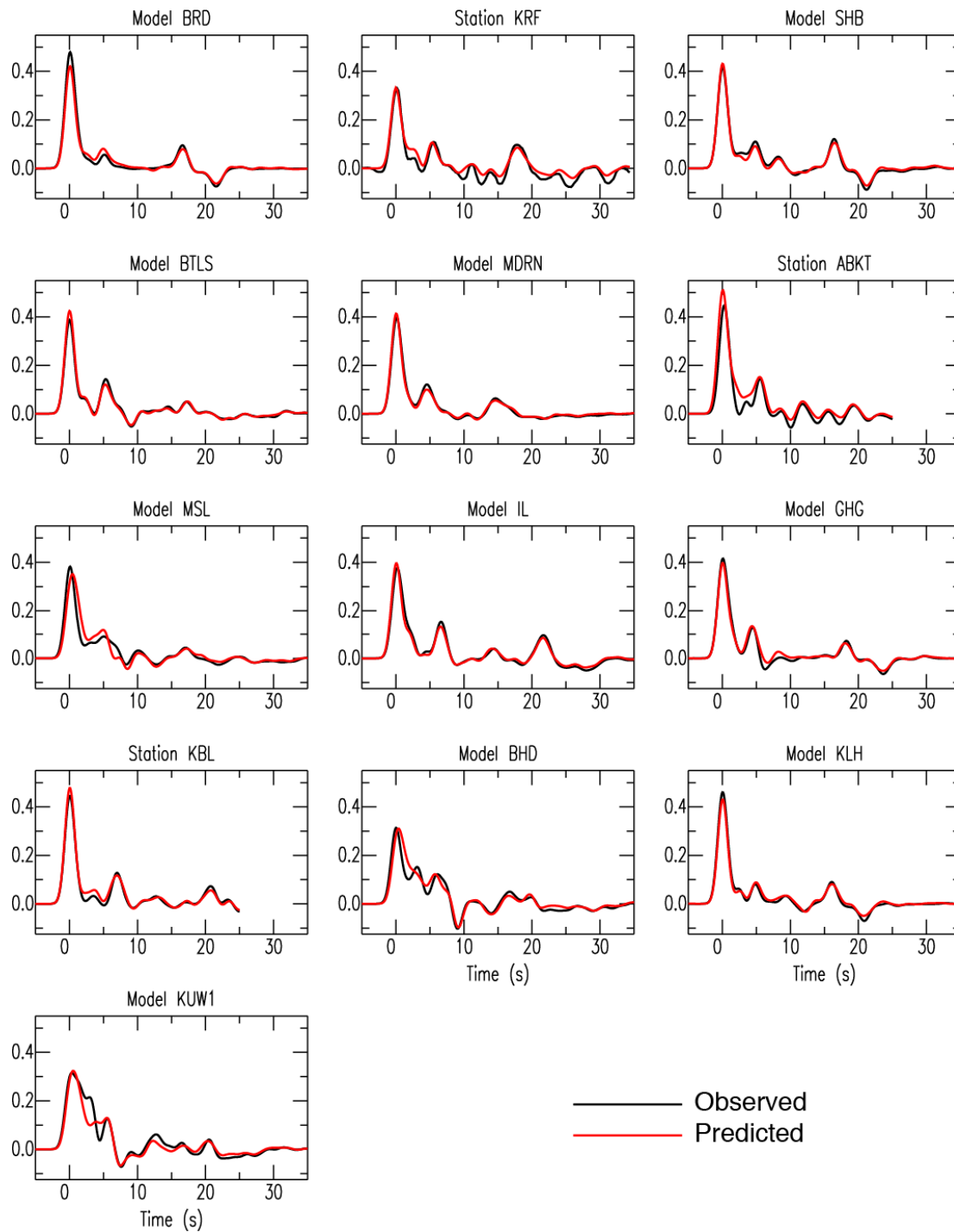


Figure 9. “Observed” and predicted radial p-wave receiver functions used in the 3D inversion. Each receiver function is associated with a single 1-degree cell. The “observed” receiver functions are actually a combination of actual observations (labeled with “Station”) and synthetic receiver functions computed using models from the literature (labeled with “Model”). The units of all the receiver functions are 1/s.

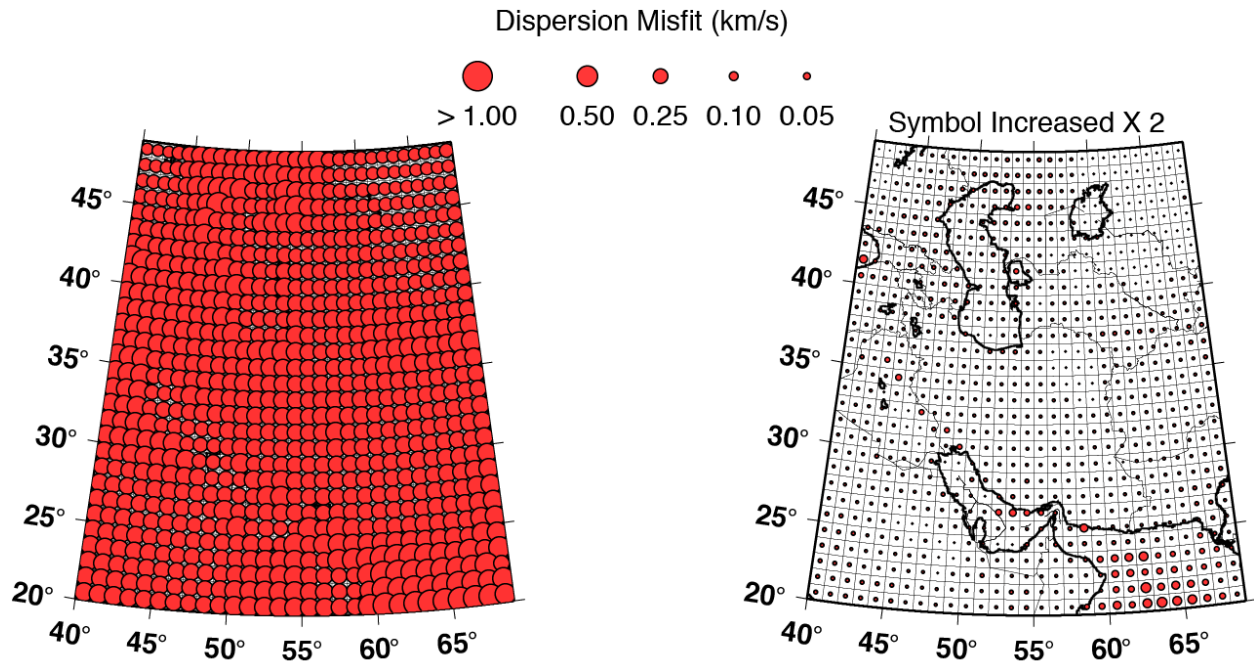


Figure 10. Initial (left) and final (after four iterations, right) dispersion misfit (Rayleigh wave phase and group velocity). The symbol size for the final misfit has been doubled so that they are more easily visible. In general, the fits are reasonable and largest offshore, and along the province boundaries, or in cells with other observations such as receiver functions that can compete for reducing misfit. However, potential systematic misfits such as matching long but not short-period observations, etc. cannot be seen with this type of display.